Åbo Akademi

OPEN ACCESS

This is an electronic reprint of the original article. This reprint may differ from the original in pagination and typographic detail.

Temperature optima of a natural diatom population increases as global warming proceeds

Hattich, G. S. I.; Jokinen, S.; Sildever, S.; Gareis, M.; Heikkinen, J.; Junghardt, N.; Segovia, M.; Machado, M.; Sjöqvist, C.

Published in:
Nature Climate Change

DOI:
10.1038/s41558-024-01981-9

Published: 08/04/2024

Document Version
Final published version

Document License
CC BY

Link to publication

Please cite the original version:
Hattich, G. S. I., Jokinen, S., Sildever, S., Gareis, M., Heikkinen, J., Junghardt, N., Segovia, M., Machado, M., & Sjöqvist, C. (2024). Temperature optima of a natural diatom population increases as global warming proceeds. *Nature Climate Change*. https://doi.org/10.1038/s41558-024-01981-9

General rights
Copyright and moral rights for the publications made accessible in the public portal are retained by the authors and/or other copyright owners and it is a condition of accessing publications that users recognise and abide by the legal requirements associated with these rights.

Take down policy
If you believe that this document breaches copyright please contact us providing details, and we will remove access to the work immediately and investigate your claim.

This document is downloaded from the Research Information Portal of ÅAU: 03. May. 2024

nature climate change

Article

https://doi.org/10.1038/s41558-024-01981-9

Temperature optima of a natural diatom population increases as global warming proceeds

Received: 27 June 2023

Accepted: 15 March 2024

Published online: 08 April 2024

Check for updates

G. S. I. Hattich[1,2], S. Jokinen[3], S. Sildever[4], M. Gareis[1], J. Heikkinen[1], N. Junghardt[1], M. Segovia[1,5], M. Machado[1,6] & C. Sjöqvist[1]

Studies in laboratory-based experimental evolution have demonstrated that phytoplankton species can rapidly adapt to higher temperatures. However, adaptation processes and their pace remain largely unknown under natural conditions. Here, by comparing resurrected *Skeletonema marinoi* strains from the Baltic Sea during the past 60 years, we show that modern *S. marinoi* have increased their temperature optima by 1 °C. With the increasing ability to grow in higher temperatures, growth rates in cold water decreased. Modern *S. marinoi* modified their valve:girdle ratio under warmer temperatures, which probably increases nutrient uptake ability. This was supported by the upregulation of several genes related to nitrate metabolism in modern strains grown under high temperatures. Our approach using resurrected strains demonstrates the adaptation potential of naturally occurring marine diatoms to increasing temperatures as global warming proceeds and exemplifies a realistic pace of evolution, which is an order of magnitude slower than estimated by experimental evolution.

The Anthropocene has moved the planet into a new human-mediated geological epoch[1], causing a rapid loss of oceanic biodiversity on a global scale[2]. The increasing average temperature is one of the most evident human-induced changes. It has wide-reaching effects on many organisms[2] due to the temperature dependency of biological processes[3]. This is especially relevant for marine organisms, as the ocean is a sink for most surplus heat[4]. Global sea surface temperature (SST) has risen by 0.7 °C and is projected to increase substantially by the end of the century[5–8]. Our study focuses on adaptation to human-induced global warming in a keystone phytoplankton species in the Baltic Sea—a region considered a 'time machine' for future ecosystem change due to experiencing warming levels above the global average[9].

Unicellular phytoplankton, accounting for 40% of global primary production[10], are essential contributors to oxygen generation, carbon sequestration and biogeochemical cycles[11], and constitute the foundation of marine food webs[12]. Distinct thermal responses of marine phytoplankton species could lead to alterations in community composition and geographical distribution with increasing SST[13]. Further, productivity and diversity are expected to decline under increasing SST if species cannot shift their distribution range or adapt to the novel environment[14]. This may be especially true for partly isolated populations as studied here[15]. However, the widespread correlation between temperature optima (T_{opt}) in phytoplankton and SST over a 150° latitudinal gradient shows that phytoplankton can adapt to different temperatures[14].

The high adaptive capacity of phytoplankton has been confirmed by experimental evolution[16], indicating rapid adaptation to new environments through selection on existing genetic diversity[17] or de novo mutations[18]. Temperature adaptation to a delta of ≥4 °C has resulted in a shift either in the T_{opt} (refs. 18–23) or the upper thermal limit[18,21,22].

[1]Environmental and Marine Biology, Åbo Akademi University, Turku, Finland. [2]Department of Biology, University of Turku, Turku, Finland. [3]Marine Geology, Geological Survey of Finland, Turku, Finland. [4]Department of Marine Systems, Tallinn University of Technology, Tallinn, Estonia. [5]Cavanilles Institute of Biodiversity and Evolution, Valencia University, Valencia, Spain. [6]Department of Animal Biology, Malaga University, Malaga, Spain. e-mail: conny.sjoqvist@abo.fi

https://doi.org/10.1038/s41558-024-01981-9

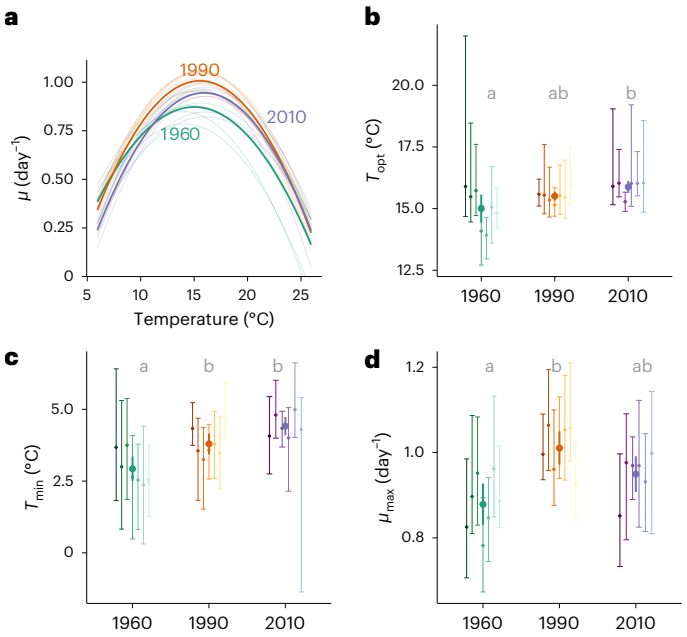

Fig. 1 | Temperature response of modern and early-Anthropocene *S. marinoi*. **a**, Mean thermal performance curves of strains from the 1960s, 1990s and 2010s (green, orange and purple, respectively). Underlying thin lines show individual performance curves of 7 strains per population. Thermal performance curves were fitted as a quadratic model. Maximum growth rate denoted by μ. **b**–**d**, Mean and confidence interval (CI) of optimum temperature (T_{opt}) (**b**), lower temperature limit (T_{min}) (**c**) and maximum growth rate (μ_{max}) (**d**) were estimated for each strain by bootstrapping ($n = 4$ replicates per strain). Overlying strain-specific responses, the mean and CI of all strains per time point and differences between time points (lowercase grey letters) are shown.

Also, increased growth and photosynthetic rates are linked to temperature adaptation[23,24]. Further, analyses of differential gene expression have revealed changes in pathways related to photosynthesis and energy metabolism[25,26]. However, the constraints on temperature adaptation, whether due to thermodynamics[6], generalist–specialist trade-offs[19] or resource allocation[22], remain a subject of ongoing debate. For example, temperature adaptation seems limited under low nitrogen concentrations[20,27]. Growth at elevated temperatures leads to an increased demand for nitrogen to sustain energetically costly repair mechanisms. This demand cannot be met under nutrient limitation because of trade-offs between allocating resources to reproduction and nutrient uptake[22]. Overall, experimental evolution studies have enhanced our understanding of phytoplankton evolution, but it remains uncertain whether the adaptive potential observed in laboratory experiments translates to real-world conditions.

Most experimental evolution studies do not include realistic selection pressures, natural diversity, interactions among individuals and species[28], or sexual reproduction, all of which can alter the adaptation potential and/or the rate of evolution. Therefore, other approaches are required for studying adaptation under real-world global warming. This is possible through a 'backward-in-time' method, by resurrecting phytoplankton resting stages from seafloor sediment archives[29–31]. A previous resurrection study using phytoplankton demonstrated a shift in life cycle processes with increasing temperatures[29]. Analysing resurrected strains provides insights into how evolutionary processes, under a natural pace of global warming, compare to evolution occurring under simulated laboratory conditions.

With increasing SST, the general expectation is that phytoplankton cells become smaller[32,33]. One postulated mechanism is that size shifts allow cells to maintain the same sinking velocity with decreasing water density at high temperatures[33]. In addition, higher temperatures can indirectly favour smaller cells through increased resource competition and reproductive rate. Smaller cells have a larger surface:volume ratio compared with larger cells and thus a larger relative area supporting resource acquisition[34], making them better competitors for resources. A shift towards smaller cells was observed in coccolithophores[18] and green algae[23] adapted to high temperatures. However, there is conflicting evidence for diatoms, with some species increasing and others decreasing in cell size in response to increasing temperature[25]. Overall, cell size decline is important to consider, as it entails the potential for far-reaching ecological consequences, including the observed productivity decline in open oceans[35].

Here we study potential temperature adaptation in a natural diatom population. We compared thermal response curves, cell size and morphology, and gene expression of resurrected early-Anthropocene (1960s) strains of the key diatom species *Skeletonema marinoi* to strains subjected to increasing global warming (1990s and 2010s). The spring-blooming marine diatom *S. marinoi* is a key primary producer in the Baltic Sea[36] and may periodically constitute up to 60–80% of the total biomass[37]. The study area in the northern Baltic Sea has been subjected to temperature increase and eutrophication during the past decades. Therefore, we expected to observe adaptation to increasing temperatures manifested as a higher T_{opt} in modern *S. marinoi* (2010s). Further, we expected to observe a shift in cell size in *S. marinoi* from the past 60 years when grown in higher temperatures, and differential gene expression of metabolic pathways that are linked to the observed shifts in thermal reaction norms and related cell-size shifts.

The temperature optima of *S. marinoi* increased over the past 60 years

Strains of *S. marinoi* isolated across the past 60 years showed a shift in temperature-dependent growth and thermal performance curves (Fig. 1). The T_{opt} of modern strains shifted by almost 1° compared with strains from the early Anthropocene (Fig. 1a,b; $F_{2,17} = 4.98$, $P = 0.019$). The mean T_{opt} of 14.99 °C in the 1960s strains shifted to 15.5 °C in the 1990s strains and increased significantly to 15.88 °C in the 2010s strains (Fig. 1b). A shift of ~1.50 °C was observed in the lower temperature limit (T_{min}; Fig. 1a,c; $F_{2,17} = 15.02$, $P < 0.001$). The strains from the 1960s showed a higher growth rate at low temperatures (Fig. 1a). Their T_{min} (2.93 °C) was significantly lower compared with the 1990s and 2010s strains (3.79 °C and 4.42 °C, respectively; Fig. 1c). No differences in the upper temperature limit (T_{max}) were observed between decades (Supplementary Fig. 5). The maximum growth rate (μ_{max}) was highest in the 1990s strains at 1.01 day^{-1}, which was 15% higher compared with the 1960s strains.

Modern *S. marinoi* display a shift in cell shape in response to increased temperature. Shifts in cell size (measured as volume) along the temperature gradient from 6–22 °C were significantly different between strains of *S. marinoi* from different decades (Fig. 2a; $F_{2,158} = 75.26$, $P < 0.001$). While the size was rather similar across temperatures in strains from the 1960s and the 1990s, the modern population increased in size by 220% from low to high temperatures. Shifts in cell size affect the surface to volume ratio of the cells, which similarly showed an interaction between the temporal populations and temperature (Fig. 2b; $F_{2,158} = 94.86$, $P < 0.001$). The response within strains from the 1960s and 1990s was similar across temperatures, while a strong decrease (40%) occurred with increasing temperatures within the strains from the 2010s. These shifts were driven by changes in cell width (Fig. 2c,d). The cell length decreased by ~30% across strains from all decades. In contrast, shifts in cell width across temperatures were dependent on the age of strains (Fig. 2b; $F_{2,158} = 77.00$, $P < 0.001$). An increase of 120% was observed within the strains from the 2010s, while strains from the 1990s and 1960s showed no shift.

https://doi.org/10.1038/s41558-024-01981-9

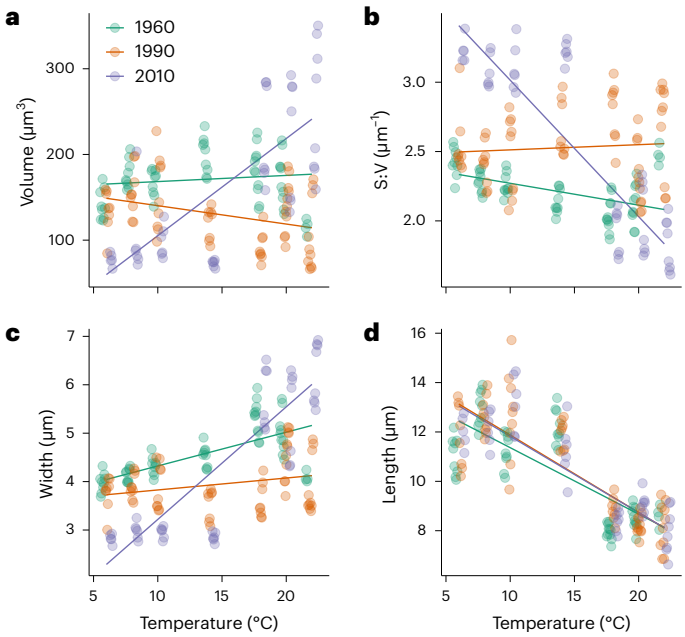

Fig. 2 | Size of modern and early-Anthropocene *S. marinoi*. **a**–**d**, Volume (**a**), surface to volume ratio (**b**; S:V), width (**c**) and length (**d**) of 3 strains from the 1960s (green), 1990s (orange) and 2 strains from the 2010s (purple). Points are the mean of 50 individual cells measured per replicate. A small jitter of data points was added around the temperature values on the *x* axis to enhance the visibility of individual measurements. Model predictions are shown as lines.

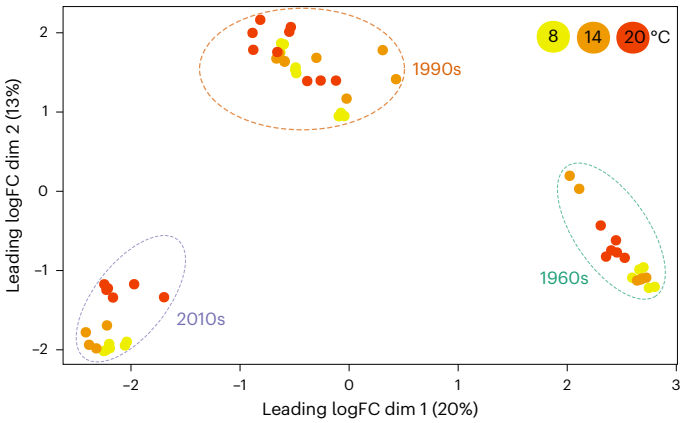

Fig. 3 | Multidimensional scaling plot displaying gene expression of the top 500 genes. Strains of *S. marinoi* from the 1960s, 1990s and 2010s in 8 °C (yellow), 14 °C (orange) and 20 °C (red). The temporal populations are highlighted by coloured dashed lines. 1960s, green; 1990s, orange; 2010s, purple.

Gene expression analysis revealed evolutionary effects on nutrient metabolism. On average, 98.2% of the RNA-seq reads per sample mapped to the *S. marinoi* reference genome (total size ~55 Mb). We observed no differences in mapping success between different strains (Supplementary Table 1). We compared potential differences in gene expression and found that in total, 8,280 of the 22,438 predicted genes were differentially expressed (DE) using a 5% false discovery rate (FDR) level. Approximately 76% or 6,328 of these DE genes (DEGs) received a functional annotation. When visualizing the top 500 DEGs, we observed a clear difference in expression patterns between strains from different time points (Fig. 3). The number of DEGs was higher between decades, when grown under the same temperature. The most pronounced difference was observed between the 1960s and the 2010s (4,948 ± 55 DEGs). This was significantly more than what was observed in the 1960s versus 1990s (4,021 ± 158) and the 1990s versus 2010s contrasts (3,532 ± 106) (*t*-test, $t = 3.18$, $P < 0.05$) (Fig. 4 and Supplementary Fig. 1).

We also observed a difference when comparing strains within time points subjected to different temperatures (Fig. 3). Between temperatures, strains from the 1960s displayed a total of 1,062 ± 138 DEGs (per strain), which is significantly less compared with that of the 1990s (1,302 ± 189) (*t*-test, $t = 2.44$, $P < 0.011$). Also, strains from the 2010s had significantly fewer DEGs (913 ± 240) between temperatures compared with strains from the 1990s (*t*-test, $t = 2.44$, $P < 0.001$) (Fig. 4). There was no difference between the 1960s and 2010s in the number of DEGs between temperatures (*t*-test, $t = 2.44$, $P = 0.643$). Especially in the 14 °C versus 20 °C and the 8 °C versus 14 °C contrasts, a low number of DEGs was observed, while a higher number of DEGs was observed in the 8 °C versus 20 °C contrast (Supplementary Fig. 2).

We consider genes that were uniquely DE in 2010s strains when comparing 8 °C to 20 °C to represent a portion of evolved functionality in *S. marinoi* (Fig. 5). There was a total of 416 such genes when including genes with log fold change (FC) values >2 or <−2. These included, for example, upregulation of thioredoxin (*Acht1*, *Acht4*), trypsin (*Loc5578510*) and one heat-shock gene (*Hsf1*) (Fig. 5). In contrast, we observed several different upregulated heat-shock genes and transcription factors (*Hsf1*, *Hsf4*, *Loc4342550*) in strains from the 1960s (Supplementary Table 2). When grouping genes with related functions into Gene Ontology (GO) terms, we observed a downregulation of functions within, for example, nicotinamide adenine dinucleotide phosphate (NADP) biosynthetic energy metabolism processes in strains from the 1990s and 2010s with increasing temperature (Fig. 6). This was not observed in strains from the 1960s. Also, differential gene expression in photosynthesis-related processes was observed in strains from the 1990s and 2010s but not seen in the 1960s strains. Mitotic sister chromatid cohesion (GO:0007064) was significantly upregulated in the 1990s and 2010s strains, which was not seen in the strains from the 1960s. In addition to shifts in these biological processes, we observed changes in related energy processes at the molecular function level (Supplementary Fig. 3). Changes to the photosynthesis machinery in modern strains were further supported by differential gene expression affecting cellular components within photosystem I and II (Supplementary Fig. 4).

Discussion

Despite mounting evidence that thermal adaptation is possible under controlled conditions[19–21,23], it remains uncertain how adaptation plays out under natural conditions. Multiple drivers including species interactions and abiotic environmental changes[27,38] can alter the selection pressure. Adaptation may also be affected by the rate of temperature change over decades and by diurnal and annual fluctuations in temperature conditions[39]. This plethora of contributing factors is essential for understanding 'real-world' selection. Here we demonstrate that a natural phytoplankton population can increase its T_{opt} apace with natural global warming over six decades. This provides evidence for a realistic pace of evolution of phytoplankton to global warming and several other metrics that have been under selection from global warming. We demonstrate that modern *S. marinoi* decreases its surface to volume ratio with increasing temperatures. This was not observed in the strains from the 1960s and 1990s. We observed shifts in how the population has altered its gene expression in relation to the increase in SST in the study area. We suggest that strains from the 1960s experienced higher temperatures as more stressful than the recent strains. This is supported by their lower growth rates in high temperatures and by a higher number of upregulated genes coding for heat-shock proteins. Heat-shock proteins are known to repair cell damage under high-temperature conditions[40]. The less-clear stress response in strains from 2010s exposed to above-optimum

https://doi.org/10.1038/s41558-024-01981-9

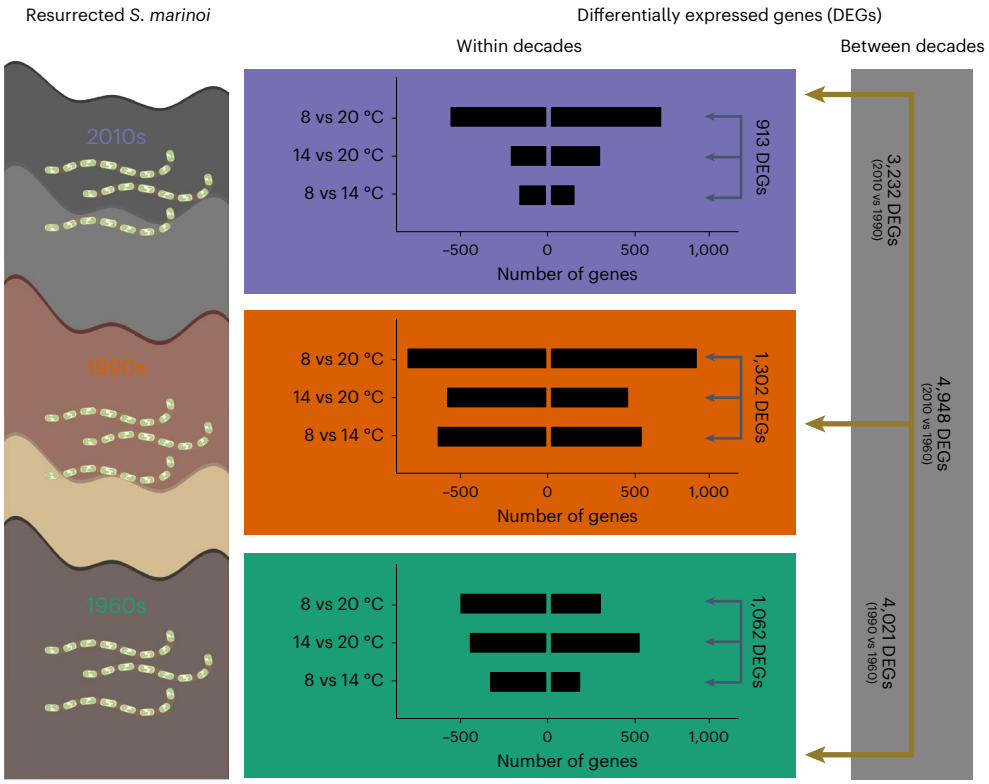

Fig. 4 | The number of DEGs (up- and downregulated) within and between decades. The strains originate from the 1960s, 1990s and 2010s across all temperature contrasts. The number of DEGs is given as mean per strain.

temperatures suggests that adaptation to ongoing climate change has already occurred.

In experimental evolution, temperature increase is frequently applied at the upper temperature limit of the species, posing a strong selective pressure. Here we have investigated the effect of a gradual increase in SST of ~1.5 °C in the study area since the 1960s. This entails a more subtle selection pressure compared with most experimental evolution studies that use a delta of ≥4 °C (refs. 19–21,23). The upper temperature tolerance limit of *S. marinoi* (>27 °C; Supplementary Fig. 5 and ref. 41) is never exceeded during the main growth season in this study area (Supplementary Fig. 6). This diverging selection pressure between experimental and natural evolution might partly explain why a comparable increase in T_{opt} required more generations in our natural population compared with populations exposed to experimental evolution. For example, *Chlamydomonas reinhardtii* exposed for a decade to +4 °C above ambient temperature in a mesocosm study showed a 1.6 °C increase in the T_{opt} (ref. 23). A comparable shift of 1–2 °C in T_{opt} was observed in two diatom species grown for 200–600 generations at 4 °C above ambient temperature[19]. Using the climatology of the sampling area and the temperature response curves, we estimate that the observed 1 °C increase in T_{opt} of *S. marinoi* required ~7,000 mitotic generations (Supplementary Fig. 6 and Supplementary Table 3). *Skeletonema marinoi* undergoes sexual reproduction and meiosis can be induced experimentally. However, it is unknown how often sexual events occur in nature[42]. Therefore, we are adhering to asexual generations in line with most laboratory evolution experiments. Also, other changing drivers in the environment (for example, light conditions and grazing), for which we have not accounted here, may have affected the population dynamics. Overall, our study demonstrates that the rate of temperature adaptation, while slower than initially estimated through experimental evolution, enables a population to adapt to ongoing global warming.

In addition, it is important to consider diurnal and seasonal temperature fluctuations, which may have contradictory effects on temperature adaptation. Diurnal fluctuations have been described to accelerate the molecular evolution of thermal tolerance in the diatom *Thalassiosira pseudonana* compared with constant exposure[39]. Further, diurnal fluctuations can lead to the evolution of plasticity[43]. Using our data in the framework of a reaction norm (as in ref. 44) suggests that the evolution of plasticity does not play a notable role in the temperature adaptation of modern strains (Supplementary Fig. 7). Seasonal temperature fluctuations may have a contradictory role by slowing down evolution. An increase in T_{opt} is often accompanied by a performance trade-off, including a reduced growth rate at low temperatures[19,22]. We observed a higher growth capacity at low temperatures in early-Anthropocene strains and a decrease in this capacity as the optimum increased. Consequently, strains with high temperature optimum favoured in late spring can have a disadvantage during cold winter seasons. The maintenance of high phenotypic diversity in isolated strains across 60 years of selection under global warming suggests temporal fluctuation in selection pressure, which favours the maintenance of high diversity[45]. Moreover, strong coupling between the pelagic population and benthic resting stages could mitigate adaptation to short-term environmental fluctuations. Benthic-pelagic coupling has been suggested to result in a homogeneous population structure across the seasons in dinoflagellates in the Baltic Sea[46]. Strong benthic-pelagic coupling has also been observed in *S. marinoi* in the study area[47,48]. Thus, it is highly unlikely that the temperature adaptation we observed was driven by seasonal or short-term fluctuations. However, increasing winter temperatures could shift the balance in favour of strains with higher T_{opt}. The selection for higher T_{opt} and reduced growth capacity at low temperatures might be one of the reasons underlying the later onset of the *S. marinoi* spring bloom observed elsewhere[49,50].

The strains isolated from the 1990s displayed the highest maximum growth rates. This may be explained by a trade-off between

https://doi.org/10.1038/s41558-024-01981-9

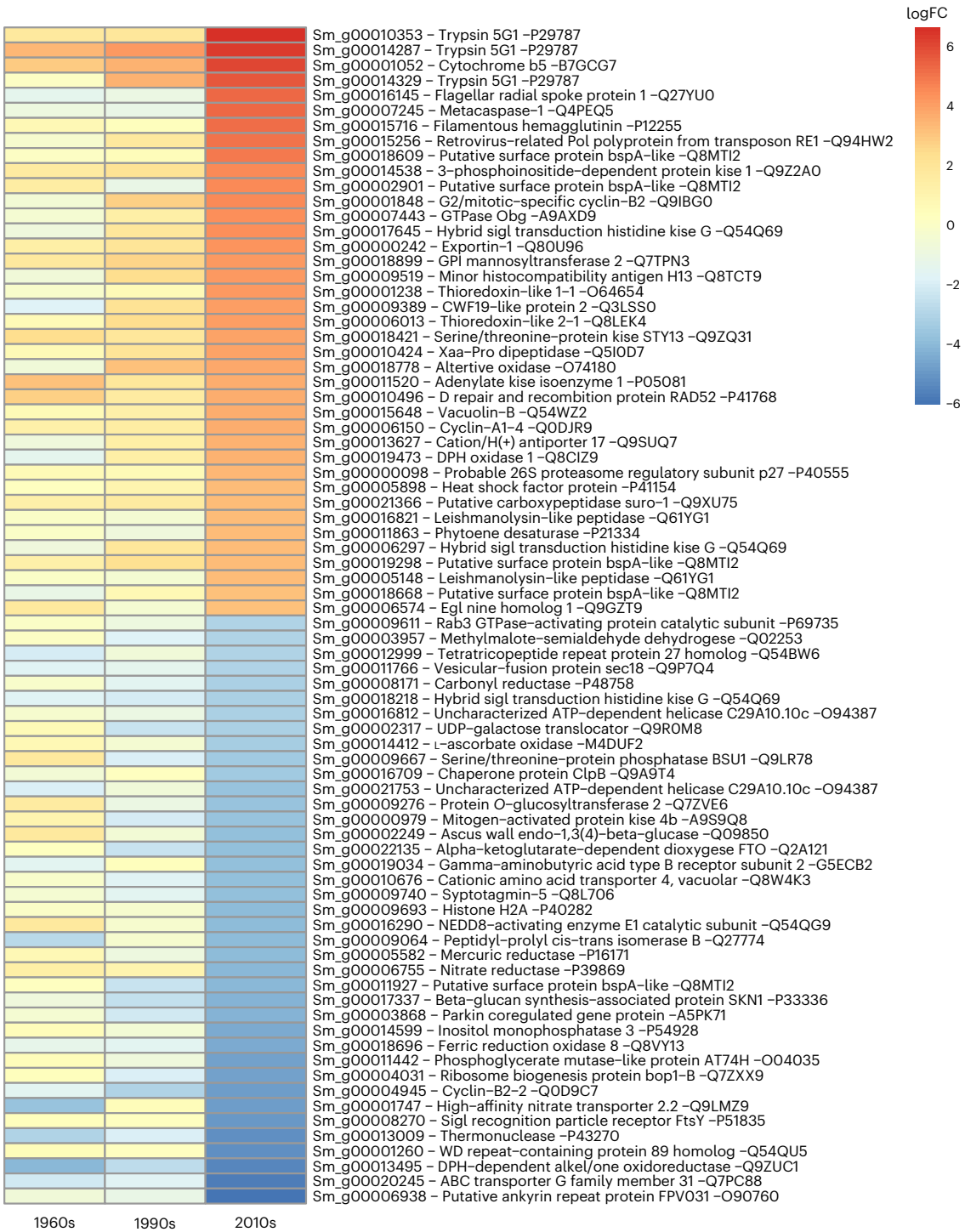

Fig. 5 | Unique DEGs in strains from the 2010s. The heatmap includes genes in strains from the 2010s that were uniquely up- or downregulated when compared at 8 °C vs 20 °C. Only the top 78 genes with logFC values >3 or <−3 are displayed.

growth and nutrient affinity. Generally, this trade-off arises as cellular resources can be allocated to reproduction or nutrient uptake[51]. The nitrogen requirement of repair mechanisms such as heat-shock proteins is expected to increase during temperature adaptation. Nitrogen limitation can thus constrain adaptation to increasing temperatures[20], making phytoplankton in areas with low nutrient conditions more vulnerable to global warming[52]. Hence, even though not directly tested here, adaptation to global warming in the population of *S. marinoi* in this study might have been enabled by the strong and documented eutrophication in the area[53]. When the limiting nutrient is present in excess, it gives individuals with higher growth a competitive advantage[54]. A higher growth rate is positively correlated with a higher maximum uptake velocity (V_{max}), which is generally observed in the velocity-adapted diatoms. These traits are advantageous under high nutrient environments[55]. In our study area, eutrophication peaked in the 1990s[9,56], which may explain the high growth rates in strains from this time. In agreement, a recent study from the Baltic Sea comparing populations of *S. marinoi* growing

https://doi.org/10.1038/s41558-024-01981-9

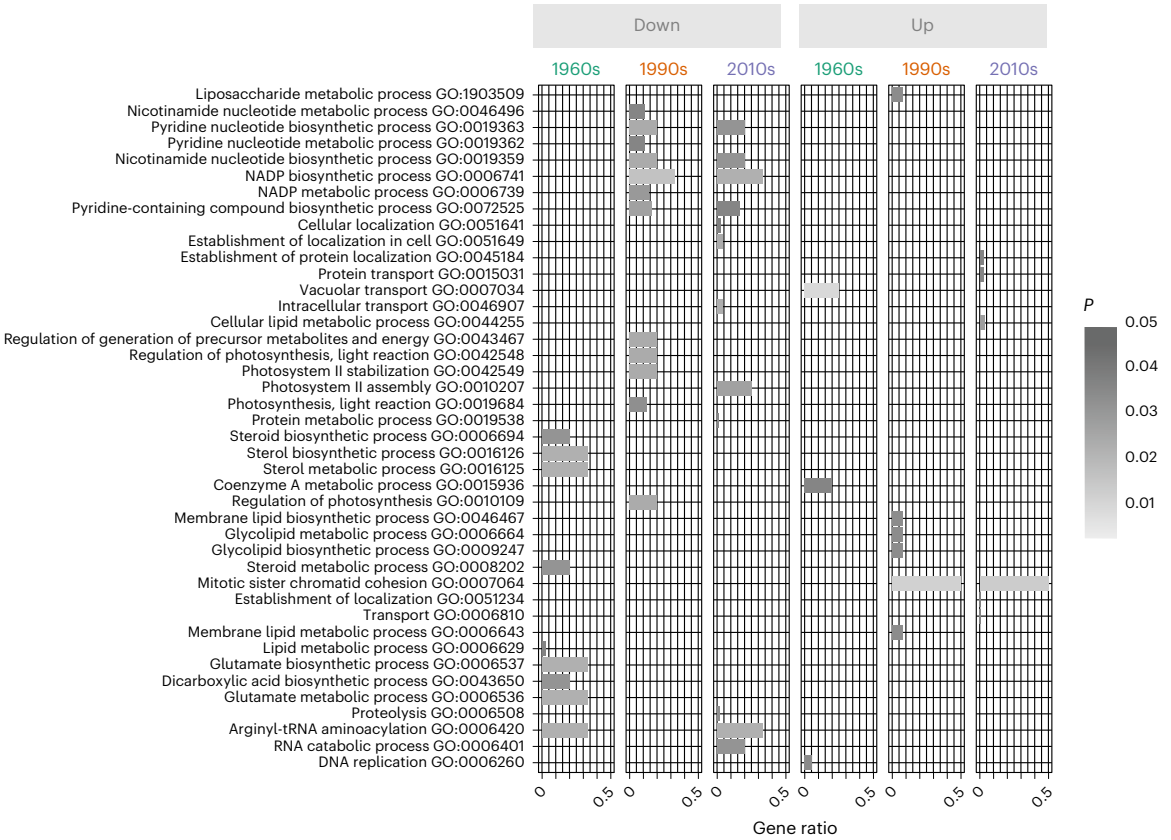

Fig. 6 | Highly significant GO terms in high temperatures. Only biological processes that were significantly up- or downregulated in a higher temperature (8 °C→14 °C, 8 °C→20 °C, 14 °C→20 °C) are represented by a bar showing the proportion of DEGs per biological process category (gene ratio). The grey scale represents the *P* value from one-tailed Fisher's exact test.

under different trophic states showed that eutrophication probably drives selection for faster growth[57]. This is further supported by the differential gene expression relating to energy metabolism and cell division (for example, GO:0046496, GO:0006739, GO:0007064). These processes are related to NADP, the central electron carrier during the light-dependent photosynthesis reactions which were most differentially expressed in strains from the 1990s and 2010s. Overall, this prompts the question of whether adaptation with ongoing global warming will be of broad applicability or if it is limited to regions subject to strong eutrophication.

Elevated temperatures tend to decrease individual cell sizes[32,33] due to resource constraints and enhanced reproductive rates. However, the silica frustules of diatoms may contribute to conflicting evidence of size changes in higher temperatures[25]. Here we show opposing responses in size and surface:volume ratio within the same species with different T_{opt}. While both early-Anthropocene and modern strains showed a reduced cell length under increasing temperatures, modern strains with higher T_{opt} showed an increase in cell width. This is in line with shifts in cell size associated with temperature evolution in the diatom *Thalassiosira pseudonana*[58]. Diatoms respond to resource limitation by adjusting the valve:girdle ratio. This ratio is relevant for nutrient acquisition, as the silica frustules restrict nutrient uptake at the elongated girdle band (length) while facilitating it at the circular valves (width) that are equipped with punctae. With increasing valve:girdle ratio, the ratio of the surface area of the valve to the volume of the cell also increased[58] (Supplementary Fig. 8) and the cell shape changed (Supplementary Fig. 9). Overall, the counterintuitive increase in size with increasing temperature adaptation is probably driven by an increased need for resources. We also found support for this higher demand for nutrients in the gene expression of modern *S. marinoi*. Among the upregulated genes in high temperature, we observed several with functions related to trypsin metabolism, which is a known regulator of N:P stoichiometric homoeostasis in phytoplankton[59]. The expression of trypsin in diatoms is especially responsive to shifts in the environment[60]. Here, it may be the key to fulfil the higher demand for nitrate when temperatures have increased and the competition for this resource simultaneously intensifies. Further, two thioredoxins, which are central regulators of CO_2 fixation and nitrogen in chloroplasts[61], were highly upregulated in strains from the 2010s. This suggests some modification of the nutrient acquisition and photosynthesis machinery in modern *S. marinoi* strains.

Conclusions

We conclude that *S. marinoi* in the Baltic Sea has adapted to ongoing global warming in the past 60 years. Our gene expression data and the observed shifts in cell morphology support earlier experimental evolution studies showing that nutrient conditions have the potential to affect adaptation to temperature increases in phytoplankton. In agreement, we also observed a trade-off between high growth at warm versus cold temperatures. However, the number of generations required by the natural population to reach the same evolutionary change was an order of magnitude greater. Overall, the underlying mechanisms of evolutionary change can be well understood in experimental studies, but the estimation of the rate of evolution requires the study of natural communities.

Online content

Any methods, additional references, Nature Portfolio reporting summaries, source data, extended data, supplementary information, acknowledgements, peer review information; details of author contributions

and competing interests; and statements of data and code availability are available at https://doi.org/10.1038/s41558-024-01981-9.

References

1. Waters, C. N. et al. The Anthropocene is functionally and stratigraphically distinct from the Holocene. *Science* **351**, aad2622 (2016).
2. McCauley, D. J. et al. Marine defaunation: animal loss in the global ocean. *Science* **347**, 1255641 (2015).
3. Mundim, K. C., Baraldi, S., Machado, H. G. & Vieira, F. M. C. Temperature coefficient (Q10) and its applications in biological systems: beyond the Arrhenius theory. *Ecol. Modell.* **431**, 109127 (2020).
4. Hoegh-Guldberg, O. & Bruno, J. F. The impact of climate change on the worlds marine ecosystems. *Science* **328**, 1523–1528 (2010).
5. Boyce, D. G., Lewis, M. R. & Worm, B. Global phytoplankton decline over the past century. *Nature* **466**, 591–596 (2010).
6. Pörtner, H.-O. et al. in *Climate Change 2014: Impacts, Adaptation, and Vulnerability* (eds Field, C. B. et al.) Ch. 6 (Cambridge Univ. Press, 2014).
7. Huang, J. et al. Recently amplified Arctic warming has contributed to a continual global warming trend. *Nat. Clim. Change* **7**, 875–879 (2017).
8. Markus Meier, H. E. et al. Climate change in the Baltic Sea region: a summary. *Earth Syst. Dyn.* **13**, 457–593 (2022).
9. Reusch, T. B. H. et al. The Baltic Sea as a time machine for the future coastal ocean. *Sci. Adv.* **4**, eaar8195 (2018).
10. Falkowski, P. G. The role of phytoplankton photosynthesis in global biogeochemical cycles. *Photosynth. Res.* **39**, 235–258 (1994).
11. Basu, S. & Mackey, K. R. M. Phytoplankton as key mediators of the biological carbon pump: their responses to a changing climate. *Sustainability* **10**, 869 (2018).
12. Cloern, J. E. Phytoplankton bloom dynamics in coastal ecosystems: a review with some general lessons from sustained investigations of San Francisco Bay, California. *Rev. Geophys.* **34**, 127–168 (1996).
13. Anderson, S. I., Barton, A. D., Clayton, S., Dutkiewicz, S. & Rynearson, T. A. Marine phytoplankton functional types exhibit diverse responses to thermal change. *Nat. Commun.* **12**, 6413 (2021).
14. Thomas, M. K., Kremer, C. T., Klausmeier, C. A. & Litchman, E. A global pattern of thermal adaptation in marine phytoplankton. *Science* **338**, 1085–1088 (2012).
15. Sjöqvist, C., Godhe, A., Jonsson, P. R., Sundqvist, L. & Kremp, A. Local adaptation and oceanographic connectivity patterns explain genetic differentiation of a marine diatom across the North Sea–Baltic Sea salinity gradient. *Mol. Ecol.* **24**, 2871–2885 (2015).
16. Reusch, T. B. H. & Boyd, P. W. Experimental evolution meets marine phytoplankton. *Evolution* **67**, 1849–1859 (2013).
17. Lohbeck, K. T., Riebesell, U. & Reusch, T. B. H. Adaptive evolution of a key phytoplankton species to ocean acidification. *Nat. Geosci.* **5**, 346–351 (2012).
18. Schluter, L. et al. Adaptation of a globally important coccolithophore to ocean warming and acidification. *Nat. Clim. Change* **4**, 1024–1030 (2014).
19. Jin, P. & Agustí, S. Fast adaptation of tropical diatoms to increased warming with trade-offs. *Sci. Rep.* **8**, 17771 (2018).
20. Aranguren-Gassis, M., Kremer, C. T., Klausmeier, C. A. & Litchman, E. Nitrogen limitation inhibits marine diatom adaptation to high temperatures. *Ecol. Lett.* **22**, 1860–1869 (2019).
21. Listmann, L., LeRoch, M., Schlueter, L., Thomas, M. K. & Reusch, T. B. H. Swift thermal reaction norm evolution in a key marine phytoplankton species. *Evol. Appl.* **9**, 1156–1164 (2016).
22. O'Donnell, D. R. et al. Rapid thermal adaptation in a marine diatom reveals constraints and trade-offs. *Glob. Change Biol.* **24**, 4554–4565 (2018).
23. Schaum, C. E. et al. Adaptation of phytoplankton to a decade of experimental warming linked to increased photosynthesis. *Nat. Ecol. Evol.* **1**, 94 (2017).
24. Padfield, D., Yvon-Durocher, Ge., Buckling, A., Jennings, S. & Yvon-Durocher, Ga. Rapid evolution of metabolic traits explains thermal adaptation in phytoplankton. *Ecol. Lett.* **19**, 133–142 (2016).
25. Liang, Y., Koester, J. A., Liefer, J. D., Irwin, A. J. & Finkel, Z. V. Molecular mechanisms of temperature acclimation and adaptation in marine diatoms. *ISME J.* **13**, 2415–2425 (2019).
26. Kontopoulos, D. G. et al. Phytoplankton thermal responses adapt in the absence of hard thermodynamic constraints. *Evolution* **74**, 775–790 (2020).
27. Aranguren-Gassis, M. & Litchman, E. Thermal performance of marine diatoms under contrasting nitrate availability. *J. Plankton Res.* **42**, 680–688 (2020).
28. Scheinin, M., Riebesell, U., Rynearson, T. A., Lohbeck, K. T. & Collins, S. Experimental evolution gone wild. *J. R. Soc. Interface* **12**, 20150056 (2015).
29. Hinners, J., Kremp, A. & Hense, I. Evolution in temperature-dependent phytoplankton traits revealed from a sediment archive: do reaction norms tell the whole story? *Proc. R. Soc. B* **284**, 20171888 (2017).
30. Härnström, K., Ellegaard, M., Andersen, T. J. & Godhe, A. Hundred years of genetic structure in a sediment revived diatom population. *Proc. Natl Acad. Sci. USA* **108**, 4252–4257 (2011).
31. Yousey, A. M. et al. Resurrected 'ancient' *Daphnia* genotypes show reduced thermal stress tolerance compared to modern descendants. *R. Soc. Open Sci.* **5**, 5172193 (2018).
32. Sommer, U., Peter, K. H., Genitsaris, S. & Moustaka-Gouni, M. Do marine phytoplankton follow Bergmann's rule sensu lato? *Biol. Rev.* **92**, 1011–1026 (2017).
33. Zohary, T., Fishbein, T., Shlichter, M. & Naselli-Flores, L. Larger cell or colony size in winter, smaller in summer – a pattern shared by many species of Lake Kinneret phytoplankton. *Inland Waters* **7**, 200–209 (2017).
34. Aksnes, D. L. & Egge, J. K. A theoretical model for nutrient uptake. *Mar. Ecol. Prog. Ser.* **70**, 65–72 (1991).
35. Boyce, D. G. & Worm, B. Patterns and ecological implications of historical marine phytoplankton change. *Mar. Ecol. Prog. Ser.* **534**, 251–272 (2015).
36. Wasmund, N. et al. Extension of the growing season of phytoplankton in the western Baltic Sea in response to climate change. *Mar. Ecol. Prog. Ser.* **622**, 1–16 (2019).
37. Jochem, F. Distribution and importance of autotrophic ultraplankton in a boreal inshore area (Kiel Bight, Western Baltic). *Mar. Ecol. Prog. Ser.* **53**, 153–168 (1989).
38. Jin, P. et al. Increased genetic diversity loss and genetic differentiation in a model marine diatom adapted to ocean warming compared to high CO_2. *ISME J.* **16**, 2587–2598 (2022).
39. Schaum, C. E., Buckling, A., Smirnoff, N., Studholme, D. J. & Yvon-Durocher, G. Environmental fluctuations accelerate molecular evolution of thermal tolerance in a marine diatom. *Nat. Commun.* **9**, 1719 (2018).
40. Macario, A. J. L. & de Macario, E. C. Molecular chaperones: multiple functions, pathologies, and potential applications. *Front. Biosci.* **12**, 2588–2600 (2007).
41. Anderson, S. I. & Rynearson, T. A. Variability approaching the thermal limits can drive diatom community dynamics. *Limnol. Oceanogr.* **65**, 1961–1973 (2020).
42. Godhe, A., Kremp, A. & Montresor, M. Genetic and microscopic evidence for sexual reproduction in the centric diatom *Skeletonema marinoi*. *Protist* **165**, 401–416 (2014).

43. Schaum, C. E., Rost, B. & Collins, S. Environmental stability affects phenotypic evolution in a globally distributed marine picoplankton. *ISME J.* **10**, 75–84 (2016).
44. Stoks, R., Govaert, L., Pauwels, K., Jansen, B. & De Meester, L. Resurrecting complexity: the interplay of plasticity and rapid evolution in the multiple trait response to strong changes in predation pressure in the water flea *Daphnia magna*. *Ecol. Lett.* **19**, 180–190 (2016).
45. Gsell, A. S. et al. Genotype-by-temperature interactions may help to maintain clonal diversity in *Asterionella formosa* (Bacillariophyceae). *J. Phycol.* **48**, 1197–1208 (2012).
46. Jerney, J. et al. Seasonal genotype dynamics of a marine dinoflagellate: pelagic populations are homogeneous and as diverse as benthic seed banks. *Mol. Ecol.* **31**, 512–528 (2022).
47. Godhe, A. & Härnström, K. Linking the planktonic and benthic habitat: genetic structure of the marine diatom *Skeletonema marinoi*. *Mol. Ecol.* **19**, 4478–4490 (2010).
48. Sefbom, J. et al. A planktonic diatom displays genetic structure over small spatial scales. *Environ. Microbiol.* **20**, 2783–2795 (2018).
49. Borkman, D. G. & Smayda, T. Multidecadal (1959–1997) changes in *Skeletonema* abundance and seasonal bloom patterns in Narragansett Bay, Rhode Island, USA. *J. Sea Res.* **61**, 84–94 (2009).
50. Lundsor, E. et al. Changes in phytoplankton community structure over a century in relation to environmental factors. *J. Plankton Res.* **44**, 866–883 (2022).
51. Klausmeier, C. A., Litchman, E., Daufreshna, T. & Levin, S. A. Optimal nitrogen-to-phosphorus stoichiometry of phytoplankton. *Nature* **429**, 171–174 (2004).
52. Thomas, M. K. et al. Temperature–nutrient interactions exacerbate sensitivity to warming in phytoplankton. *Glob. Change Biol.* **23**, 3269–3280 (2017).
53. Voss, M. et al. History and scenarios of future development of Baltic Sea eutrophication. *Estuar. Coast. Shelf Sci.* **92**, 307–322 (2011).
54. Litchman, E., Klausmeier, C. A., Schofield, O. M. & Falkowski, P. G. The role of functional traits and trade-offs in structuring phytoplankton communities: scaling from cellular to ecosystem level. *Ecol. Lett.* **10**, 1170–1181 (2007).
55. Sommer, U. The paradox of the plankton: fluctuations of phosphorus availability maintain diversity of phytoplankton in flow-through cultures. *Limnol. Oceanogr.* **29**, 633–636 (1984).
56. Gustafsson, B. G. et al. Reconstructing the development of Baltic Sea eutrophication 1850–2006. *Ambio* **41**, 534–548 (2012).
57. Olofsson, M., Almen, A. K., Jaatinen, K. & Scheinin, M. Temporal escape-adaptation to eutrophication by *Skeletonema marinoi*. *FEMS Microbiol. Lett.* **369**, fnac011 (2022).
58. O'Donnell, D. R., Beery, S. M. & Litchman, E. Temperature-dependent evolution of cell morphology and carbon and nutrient content in a marine diatom. *Limnol. Oceanogr.* **66**, 4334–4346 (2021).
59. You, Y. et al. Trypsin is a coordinate regulator of N and P nutrients in marine phytoplankton. *Nat. Commun.* **13**, 4022 (2022).
60. You, Y., Sun, X. & Lin, S. An ancient enzyme finds a new home: prevalence and neofunctionalization of trypsin in marine phytoplankton. *J. Phycol.* **59**, 152–166 (2023).
61. Kikutani, S. et al. Redox regulation of carbonic anhydrases via thioredoxin in chloroplast of the marine diatom *Phaeodactylum*. *J. Biol. Chem.* **287**, 20689–20700 (2012).

Publisher's note Springer Nature remains neutral with regard to jurisdictional claims in published maps and institutional affiliations.

Open Access This article is licensed under a Creative Commons Attribution 4.0 International License, which permits use, sharing, adaptation, distribution and reproduction in any medium or format, as long as you give appropriate credit to the original author(s) and the source, provide a link to the Creative Commons licence, and indicate if changes were made. The images or other third party material in this article are included in the article's Creative Commons licence, unless indicated otherwise in a credit line to the material. If material is not included in the article's Creative Commons licence and your intended use is not permitted by statutory regulation or exceeds the permitted use, you will need to obtain permission directly from the copyright holder. To view a copy of this licence, visit http://creativecommons.org/licenses/by/4.0/.

© The Author(s) 2024

Methods

Model organism

The spring bloom in the northeast Baltic Sea is often dominated by the marine diatom *S. marinoi* which serves as an important food source for zooplankton[37]. This model species has been extensively studied in terms of biogeography, physiology and genetic variation across space and time in temperate areas of the world[62,63]. It is known to form resting stages that sink to the seafloor when the bloom phase is over towards the end of the spring bloom[64]. This 'biological archive' may contain up to ~57,000 *S. marinoi* cells per gram sediment[64], with the potential to reveal the diversity and ecophysiology of past populations.

Study area, sediment sampling and age modelling

The Småholmen station (60.24° N, 22.04° E) close to Haverö in the Archipelago Sea is 20 m deep and has been seasonally anoxic or hypoxic at the seafloor for at least seven decades[65]. The low oxygen conditions and lack of bioturbation have resulted in the formation of laminated sediment at this site. Such conditions are optimal for preserving the chronology of sedimented cells. Historical data show that the average spring temperature (air) in the Archipelago Sea was stable at ~2 °C from the 1880s until the 1970s. Since the mid-1970s, it has increased by ~0.5 °C per decade[66]. An increase in the SST has been observed close to our study site (Seili monitoring station located <3 km from Småholmen). In April, when the spring bloom reaches its peak, SST has increased by ~2.5 °C since the early 1980s (Supplementary Fig. 10).

Sediment cores were retrieved in April 2020 using an HTH Kajak surface sediment gravity corer[67] at the Småholmen station. After core retrieval, the core tube containing undisturbed sediment profiles was attached to a stand on-site and carefully sliced into 2 cm subsamples. The outer edge (3 cm) of the entire sediment core was discarded to avoid cross-contamination between different depth layers due to smearing along the outer edge of the core. The subsamples were stored in the dark at 8 °C until further processing. An age–depth model for the sediment core was constructed with the Undatable software[68] using an xfactor of 0.1 and 15% bootstrapping (Supplementary Fig. 11). The xfactor value determines the sediment accumulation rate uncertainty between consecutive age–depth constraints and the bootstrapping function randomly removes a selected percentage of the age–depth constraints in each run of the age–depth simulation[68]. Age constraints for the modelling procedure were obtained through loss on ignition (LOI) correlation against previous studies in the same location[47]. LOI was determined at 2 cm intervals by drying the subsamples at 105 °C for 16 h and ashing at 550 °C for 2 h. The LOI correlation was further verified by ^{137}Cs dating of a replicate sediment core retrieved for this study (Supplementary Fig. 12). For this, ^{137}Cs activity of the untreated 2-cm-thick sediment slices was determined by gamma spectrometry using a BrightSpec bMCA-USB pulse height analyser coupled to a well-type NaI(Tl) detector[69]. In the northern hemisphere, ^{137}Cs contamination in sediments is mainly derived from the Chernobyl nuclear power plant accident in 1986 and atmospheric nuclear weapons testing in the early 1960s[70]. Therefore, the ^{137}Cs dating of Baltic Sea sediments is based on the recognition of these two horizons in the sediment profiles.

Resurrection of clonal cultures

Resurrection was initiated by mixing 0.5 g of sediment from different layers with each 50 ml of filtered (0.22 µm) seawater with f/2+Si medium[71] in June 2020. The sediment was from the 2–4 cm, 28–30 cm and 46–48 cm layers corresponding to median age ± 1σ error estimates of 2017–2019–2020 (referred to as ~2010s/modern), 1985–1992–2001 (~1990s) and 1957–1963–1969 (~1960s/early Anthropocene), respectively (Supplementary Fig. 8). The sediment 'slurries' were distributed on 24-well NUNC plates and incubated at 8 °C and 40 µmol photons m^{-2} s^{-1} (12 h:12 h light:dark cycle). When vegetative growth emerged (after 2–4 weeks), single chains of *S. marinoi* were isolated using a micropipette under an inverted light microscope (Nikon Diaphot 300). One chain per well was isolated to a new well to minimize the probability of isolating the same clone twice. As previous population genetic studies on *S. marinoi* have shown, the genotypic diversity of *S. marinoi* is extremely high[72]. Thus, it is highly unlikely to ever find the same genotype (using, for example, microsatellite markers) of this species in natural conditions when sampled over time or across space. Therefore, we considered that the strains included in this study were all different genotypes and consisted of a small percentage of the population's total intraspecific diversity. The isolated strains can theoretically stem from different seasons, as each layer contains resting stages across seasons from 2–5 years. We confirmed that the strains belonged to the species *S. marinoi* by sequencing the V4 region of the 18S ribosomal RNA gene (for more details see Supplementary Information, 'Genetic identification of *S. marinoi*'). After 1–2 weeks, the entire volume in each well was transferred to 40 ml culture flasks containing 10 ml of f/2+Si media. After further growth for 7 days, the total volume was increased to 40 ml, and clonal cultures were maintained in the same conditions as described above. The resurrection rate varied between 44 and 58% (isolated cells that made it to a stable culture). The rates for the 1960s, 1990s and 2010s were 52%, 58% and 44%, respectively.

Experiments

To test whether *S. marinoi* has adapted to an increase in temperature during the past ~60 years, we assayed seven strains per time point (1960s, 1990s, 2010s) in +6 °C, +8 °C, +10 °C, +14 °C, +18 °C, +20 °C, +22 °C and +26 °C in natural seawater (6 PSU, 0.22 µm filtered, with f/4+Si) and 100 µmol photons m^{-2} s^{-1} (12 h:12 h light:dark cycle). Due to technical limitations, each temperature was assessed in a separate experiment in a randomized order (Supplementary Table 4). Randomization minimizes the influence of measurement timing on different temperature treatments by ensuring that the timing effect is evenly distributed across the temperature range. Before each experimental start, strains were acclimated to f/4+Si media for 1 week. The experiment was started by transferring cells to new media, reaching a start concentration of 10,000 cells per ml. To avoid dilution of nutrients, the maximum inoculum was 5 ml (10% of the total volume). The growth of each strain (four replicates) was monitored daily by measuring the in vivo fluorescence of chlorophyll *a* in a 300 µl subsample on a 96-well plate (PerkinElmer, IsoPlate 96F) using a spectrophotometer (Tecan, Infinite 200 Pro with the software Magellan for Tecan Infinite Pro v.1) until the stationary phase was reached. The excitation wavelength was set to 425 nm and the emission wavelength to 680 nm. To account for uneven distribution of cells, nine positions were measured in each well. The cells were not dark-adapted, but to mitigate potential confounding effects of light adaptation during the diurnal light–dark cycle, measurements were consistently taken at the same time. At the end of the experiment, 1 ml subsamples were fixed with acidic Lugol's solution for later estimation of cell size. Three randomly chosen strains from each time point were consistently sampled for RNA when the stationary phase was reached (Supplementary Table 5). About 25–35 ml of cell culture was centrifuged for 30 min at 4 °C at 3,900 × *g* (Eppendorf, 5810R). The cell pellet was resuspended in 400 µl of TRIzol (Invitrogen) and incubated for 2 min at 60 °C until completely dissolved. The cells were immediately stored at −80 °C until RNA extraction.

Thermal performance curves based on growth

Growth was calculated by fitting a linear model ('easy_linear') to blank-corrected fluorescence values using the 'growthrate' package[73] in R (v.4.3.0)[74] and R Studio (v.2023.9.0.463)[75]. We excluded all replicates that showed negative growth (all replicates in 26 °C, 1960_05/06 in 22 °C) or unstable growth (maximum fluorescence <2,000) before fitting the growth model. For the samples with negative growth, the growth rate was set to zero for further analysis. Strain 2010_13 was potentially contaminated and was excluded from all downstream analyses. The calculated growth rates (total *n* of 216, 222 and 184 for

the 1960s,1990s and 2010s, respectively) were plotted against temperature and thermal performance curves fitted using the 'rTPC' package[24]. The best-fitting model was chosen using the mean growth rate per temperature for each time point (1960s, 1990s, 2010s). Based on the Akaike information criterion (AIC) and the Bayesian information criterion (BIC), the best-fitting model was quadratic (models included: beta_2012, Gaussian, quadratic, Thomas_2012, Thomas_2017, Weinbull_1995). For each strain, confidence intervals of estimated parameters were produced by bootstrapping (maximum of 999 iterations). Bootstrapping simulated datasets from the existing data (including all four replicates) by sampling with replacement. Differences in estimated parameters such as T_{opt}, T_{min} and μ_{max} between strains from different time points were tested using a Tukey's HSD (honestly significant difference, two-sided). The T_{max} was excluded as a primary response since (1) *S. marinoi* rarely occurs in the region during summer when the temperature conditions may reach levels close to or above their T_{max} and (2) our attempt to capture the decline in growth rates at elevated temperatures was partly unsuccessful, leading to high uncertainty in the T_{max} estimates.

Estimating cell size

We measured cell size for a subset of three strains from each time point. Lugol-fixed samples were settled for 15 min in a Sedgewick–Rafter counting chamber. Using an inverted Olympus IX 51 microscope and an Olympus U-CMAD3 digital camera, a minimum of 10 pictures per sample were taken under ×200 magnification. The width and height of five cells were measured from each picture (Olympus cellSens Dimension imaging software v.3.2). The cells were chosen randomly and only one cell per chain was measured to include the natural variability present between the chains. The silicaceous marginal processes connecting the cells were not included in the width measurements as it was not always possible to determine where the process of the next cell started. For each cell, we calculated the size as biovolume and the surface area following the formula given in ref. 76. From this, we calculated the ratio of surface area to volume (S:V). We analysed differences in volume, S:V ratio, width and length using a linear mixed effect model (LME) including genotypes nested by age of the population as a random effect lme (Volume/SV/Width/Length ~Age+temp+Age:temp+(1|Genotype:Age)). The models were fitted using the 'lme4' package[77] in R and visualized using 'lmerTest'[78] and 'ggplot2'[79].

RNA extraction and sequencing

RNA was extracted with the RNeasy plant mini kit (Qiagen) according to manufacturer instructions with some modifications. TRIzol was removed from samples thawed on ice before extraction by centrifuging for 10 min at 8 °C at 4,500 × *g*. The cell pellet was washed once with nuclease-free water before proceeding with the extraction. RLT lysis buffer was added to the washed cell pellet without any additional mechanical lysis steps before proceeding with the extraction protocol according to manufacturer instructions. The quality of the RNA extracts was ensured using an Agilent Bioanalyzer 2100. Sequencing was performed on samples from the 8 °C, 14 °C and 20 °C experiments with three of the biological replicates per strain, except in cases of insufficient RNA yield (Supplementary Table 5). The library was prepared according to the Illumina Stranded mRNA library preparation protocol using 100 ng of RNA per sample as the starting material. Stranded mRNA sequencing was performed using Illumina NovaSeq 6000 (S4 v.1.5), producing ~90 million paired-end reads (2 × 150 bp) per sample.

RNA-seq data analysis

The quality of read pairs from all 60 samples was checked using FastQC (v.0.11.8)[80]. Only light read trimming from the '3 ends was conducted using Trimmomatic (TRAILING:20) to ensure a minimum (≥20) Phred33 score also towards the end of each sequence where the base quality normally drops in Illumina sequences. Since read trimming may lead to short reads and subsequent spurious alignment to the reference genome downstream, we required a minimum sequence length of 50 after trimming (MINLEN:50)[81]. Reads were aligned to the *S. marinoi* reference genome (https://zenodo.org/records/7786015) using BWA (v.0.7.17)[82] (Supplementary Table 1). The resulting '.bam' files were sorted and indexed using Samtools (v.1.16.1)[83]. Count tables for individual samples were created using Samtools, resulting in several mapped reads per predicted gene. The model fitting was conducted in edgeR[84]. First, the count tables were filtered using the count per million (CPM) so that only genes with at least one CPM in at least three samples were retained. The count data were normalized using a set of normalization factors (one for each sample) to eliminate composition biases between libraries. We explored the expression profiles of individual samples more closely by generating mean-difference plots (Supplementary Fig. 13). Before the differential gene expression analysis was conducted, we estimated the dispersion (Supplementary Fig. 14) and accounted for gene-specific variability from both biological and technical sources by fitting the actual model with the glmQLFit function (Supplementary Fig. 15). We calculated the leading FC by taking the root mean square of the largest 500 $\log_2$FC between pairwise samples to explore general patterns in the entire data set. For the analysis of differential gene expression, we defined different contrasts of interest. First, we analysed differences in gene expression of each strain across three temperatures (8 °C, 14 °C and 20 °C). Second, we assessed whether the mean change in gene expression across temperatures was comparable between the 1960s, 1990s and 2010s. To test whether any of the contrasts were significant (controlling for the gene-level FDR), we performed a stage-wise testing procedure in stageR[85]. This consisted of a screening stage and a confirmation stage conducted as in ref. 86. In total, 102 genes that were identified as significant in the screening stage were removed after the confirmation stage. We continued the analyses with 8,280 genes that displayed significant *P* values after FDR adjustment (alpha level 5%; Supplementary Fig. 1). Differences in the number of DEGs between decades and across temperatures were analysed using a Student's *t*-test (two-sided).

The functional annotation of the *S. marinoi* genome was conducted using different tools. Briefly, we used BLAST+ (v.2.13.0)[87] to run sequence similarity blastp searches of all *S. marinoi* proteins annotated in the genome against the Swissprot database. We retained the best hit using a maximum *e*-value limit of 1×10^{-6}. InterProScan (5.55–88.0)[88] was used to acquire GO terms and Pfam domains. In addition, we obtained KEGG pathway annotations using the web version of KofamKOALA[89]. For a gene to be considered functionally annotated, we required hits in the SwissProt database and that it received at least one assignment to Pfam domains, GO and/or KEGG annotation. GO enrichment was done with TopGO (over-representation analysis)[90] and revealed the biological processes, molecular functions and cellular components the DEGs were linked to. We conducted GO enrichment tests for genes that were up- or downregulated in high temperatures based on the mean response. We used REVIGO[91] to remove redundant GO terms.

Reporting summary

Further information on research design is available in the Nature Portfolio Reporting Summary linked to this article.

Data availability

All RNA sequence data produced in this study can be accessed through the National Center for Biotechnology Center (NCBI) under the BioProject code PRJNA1016074 and Sequence Read Archives (SRA) SRR26046577–SRR26046596. All *S. marinoi* strains are publicly available from the authors. All other experimental data are available via Zenodo at https://doi.org/10.5281/zenodo.10731675 (ref. 92). The Swissprot database (https://www.ebi.ac.uk/uniprot/download-center) was downloaded on 3 April 2023. We used the KofamKOALA version of 3 April 2023 (KEGG release 106.0).

References

62. Kooistra, W. H. C. F. et al. Global diversity and biogeography of *Skeletonema* species (Bacillariophyta). *Protist* **159**, 177–193 (2008).
63. Saravanan, V. & Godhe, A. Genetic heterogeneity and physiological variation among seasonally separated clones of *Skeletonema marinoi* (Bacillariophyceae) in the Gullmar Fjord, Sweden. *Eur. J. Phycol.* **45**, 177–190 (2010).
64. McQuoid, M. R., Godhe, A. & Nordberg, K. Viability of phytoplankton resting stages in the sediments of a coastal Swedish fjord. *Eur. J. Phycol.* **37**, 191–201 (2002).
65. Jokinen, S. A. et al. A 1500-year multiproxy record of coastal hypoxia from the northern Baltic Sea indicates unprecedented deoxygenation over the 20th century. *Biogeosciences* **15**, 3975–4001 (2018).
66. Laakso, L. et al. 100 years of atmospheric and marine observations at the Finnish Utö Island in the Baltic Sea. *Ocean Sci.* **14**, 617–632 (2018).
67. Renberg, I. & Hansson, H. The HTH sediment corer. *J. Paleolimnol.* **40**, 655–659 (2008).
68. Lougheed, B. C. & Obrochta, S. P. A rapid, deterministic age-depth modeling routine for geological sequences with inherent depth uncertainty. *Paleoceanogr. Paleoclimatol.* **34**, 122–133 (2019).
69. Ojala, A. E. K., Luoto, T. P. & Virtasalo, J. J. Establishing a high-resolution surface sediment chronology with multiple dating methods – testing ^{137}Cs determination with Nurmijärvi clastic-biogenic varves. *Quat. Geochronol.* **37**, 32–41 (2017).
70. Kotilainen, A. T., Kotilainen, M. M., Vartti, V. P., Hutri, K. L. & Virtasalo, J. J. Chernobyl still with us: ^{137}Caesium activity contents in seabed sediments from the Gulf of Bothnia, northern Baltic Sea. *Mar. Pollut. Bull.* **172**, 112924 (2021).
71. Guillard, R. R. L. in *Culture of Marine Invertebrate Animals* (eds Smith, W. L. & Chanley, M. H.) 29–60 (Springer, 1975).
72. Sassenhagen, I., Erdner, D. L., Lougheed, B. C., Richlen, M. L. & Sjöqvist, C. Estimating genotypic richness and proportion of identical multi-locus genotypes in aquatic microalgal populations. *J. Plankton Res.* **44**, 559–572 (2022).
73. Petzoldt, T. growthrates: Estimate Growth Rates from Experimental Data. R package version 0.8.4. *GitHub* https://github.com/tpetzoldt/growthrates (2022).
74. R Core Team. *R: A Language and Environment for Statistical Computing* (R Foundation for Statistical Computing, 2022).
75. RStudio Team. RStudio: Integrated Development Environment for R. *RStudio, PBC* http://www.rstudio.com/ (2020).
76. Hillebrand, H., Dürselen, C.-D., Kirschtel, D., Pollingher, U. & Zohary, T. Biovolume calculation for pelagic and benthic microalgae. *J. Phycol.* **424**, 403–424 (1999).
77. Douglas, B., Mächler, M., Bolker, B. & Walker, S. Fitting linear mixed-effects models using lme4. *J. Stat. Softw.* **67**, 1–48 (2015).
78. Kuznetsova, A., Brockhoff, P. B. & Christensen, R. H. B. lmerTest package: tests in linear mixed effects models. *J. Stat. Softw.* **82**, 1–26 (2017).
79. Wickham, H. *ggplot2: Elegant Graphics for Data Analysis* (Springer, 2009).
80. Andrews, S. FastQC: A Quality Control Tool for High Throughput Sequence Data. *Babraham Bioinformatics* https://www.bioinformatics.babraham.ac.uk/projects/fastqc/ (2010).
81. Williams, J. L., Kendall, B. E. & Levine, J. M. Experimental landscapes. *Science* **353**, 482–485 (2016).
82. Li, H. & Durbin, R. Fast and accurate short read alignment with Burrows–Wheeler transform. *Bioinformatics* **25**, 1754–1760 (2009).
83. Danecek, P. et al. Twelve years of SAMtools and BCFtools. *Gigascience* **10**, giab008 (2021).
84. Robinson, M. D., McCarthy, D. J. & Smyth, G. K. edgeR: a Bioconductor package for differential expression analysis of digital gene expression data. *Bioinformatics* **26**, 139–140 (2009).
85. Van den Berge, K., Soneson, C., Robinson, M. D. & Clement, L. stageR: a general stage-wise method for controlling the gene-level false discovery rate in differential expression and differential transcript usage. *Genome Biol.* **18**, 151 (2017).
86. Pinseel, E. et al. Strain-specific transcriptional responses overshadow salinity effects in a marine diatom sampled along the Baltic Sea salinity cline. *ISME J.* **16**, 1776–1787 (2022).
87. Altschul, S. F., Gish, W., Miller, W., Myers, E. W. & Lipman, D. J. Basic local alignment search tool. *J. Mol. Biol.* **215**, 403–410 (1990).
88. Jones, P. et al. InterProScan 5: genome-scale protein function classification. *Bioinformatics* **30**, 1236–1240 (2014).
89. Aramaki, T. et al. KofamKOALA: KEGG Ortholog assignment based on profile HMM and adaptive score threshold. *Bioinformatics* **36**, 2251–2252 (2020).
90. Alexa, A. & Rahnenfuhrer, J. topGO: Enrichment Analysis for Gene Ontology. R package version 2.52.0. *Bioconductor* https://bioconductor.org/packages/topGO (2023).
91. Supek, F., Bošnjak, M., Škunca, N. & Šmuc, T. Revigo summarizes and visualizes long lists of gene ontology terms. *PLoS ONE* **6**, e21800 (2011).
92. Hattich, G. S. I. et al. Temperature optima of a natural diatom population increases as global warming proceeds. *Zenodo* https://doi.org/10.5281/zenodo.10731675 (2024).

Acknowledgements

This research was funded by the Academy of Finland (grant number 321609) (C.S.), the Swedish Cultural Foundation (grant number 176762) (C.S.), the European Regional Development Fund and the programme Mobilitas Pluss (MOBTP160) (M.S., M.M.), the Estonian Research Council (grant PSG735) (S.S.), the Finnish Society of Sciences and Letters (G.S.I.H.), the Deutsche Forschungsgemeinschaft (DFG, German Research Foundation; HA 9696/1-1) (G.S.I.H.) and the Åbo Akademi University Foundation (C.S.). This study utilized research infrastructure as part of the FINMARI consortium (Finnish Marine Research Infrastructure network) and was supported by the molecular lab at Husö Biological Station, Finnish Functional Genomics Centre, Turku Bioscience, Åbo Akademi University and the University of Turku. Open access fees were covered by Gösta Branders research fund, Åbo Akademi Research Foundation. We also acknowledge CSC – IT Center for Science, Finland, for computational resources; K. Künnis-Beres, K. Pärt and L. Lattu for the measurement of cell sizes; P. Kallio for support with the spectrophotometer; and K. Ramesh for proofreading the paper.

Author contributions

C.S. conceived the presented idea. Sediment cores were taken by C.S., M.G. and S.J. Sediment cores were dated by S.J. and M.G. M.G., C.S., G.S.I.H. and S.S. designed the experiment. Experimental work was carried out by M.G., J.H., N.J., M.S. and M.M. Cell-size measurements were conducted by S.S. C.S., G.S.I.H. and S.J. analysed the data. G.S.I.H. and C.S. wrote the paper, and all other authors revised the paper and gave final approval for publication.

Competing interests

The authors declare no competing interests.

Additional information

Supplementary information The online version contains supplementary material available at https://doi.org/10.1038/s41558-024-01981-9.

Correspondence and requests for materials should be addressed to C. Sjöqvist.

Peer review information *Nature Climate Change* thanks Peng Jin, Daniel R. O'Donnell and the other, anonymous, reviewer(s) for their contribution to the peer review of this work.

Reprints and permissions information is available at www.nature.com/reprints.

nature portfolio

Corresponding author(s): Sjöqvist, Conny

Last updated by author(s): Feb 28, 2024

Reporting Summary

Nature Portfolio wishes to improve the reproducibility of the work that we publish. This form provides structure for consistency and transparency in reporting. For further information on Nature Portfolio policies, see our Editorial Policies and the Editorial Policy Checklist.

Statistics

For all statistical analyses, confirm that the following items are present in the figure legend, table legend, main text, or Methods section.

n/a	Confirmed	
☐	☒	The exact sample size (*n*) for each experimental group/condition, given as a discrete number and unit of measurement
☐	☒	A statement on whether measurements were taken from distinct samples or whether the same sample was measured repeatedly
☐	☒	The statistical test(s) used AND whether they are one- or two-sided *Only common tests should be described solely by name; describe more complex techniques in the Methods section.*
☐	☒	A description of all covariates tested
☐	☒	A description of any assumptions or corrections, such as tests of normality and adjustment for multiple comparisons
☐	☒	A full description of the statistical parameters including central tendency (e.g. means) or other basic estimates (e.g. regression coefficient) AND variation (e.g. standard deviation) or associated estimates of uncertainty (e.g. confidence intervals)
☐	☒	For null hypothesis testing, the test statistic (e.g. *F*, *t*, *r*) with confidence intervals, effect sizes, degrees of freedom and *P* value noted *Give P values as exact values whenever suitable.*
☒	☐	For Bayesian analysis, information on the choice of priors and Markov chain Monte Carlo settings
☒	☐	For hierarchical and complex designs, identification of the appropriate level for tests and full reporting of outcomes
☒	☐	Estimates of effect sizes (e.g. Cohen's *d*, Pearson's *r*), indicating how they were calculated

Our web collection on statistics for biologists contains articles on many of the points above.

Software and code

Policy information about availability of computer code

Data collection	These software were used for data collection: Magellan for Tecan Infinite Pro spectrophotometer v1, Olympus cellSens Dimension imaging software (version 3.2)
Data analysis	All data and code is available here, 10.5281/zenodo.10101463. These software and R packages were used for the data analysis: R (version 4.3.0), R Studio (version 2023.9.0.463), Undatable software (version 1.31), FastQC v.0.11.8, Trimmomatic v.0.39, BWA v.0.7.17, Samtools v.1.16.1, BLAST+ v2.13.0, KofamKOALA, REVIGO v.1.8.1 , R packages: growthrate v.1.3, rTPC v.1.0.4, lme4 v.1.1-31, lmerTest v3.1-3, ggplot2 v3.4.0, edgeR v.3.40.0, stageR v.1.20

For manuscripts utilizing custom algorithms or software that are central to the research but not yet described in published literature, software must be made available to editors and reviewers. We strongly encourage code deposition in a community repository (e.g. GitHub). See the Nature Portfolio guidelines for submitting code & software for further information.

Data

Policy information about availability of data

All manuscripts must include a data availability statement. This statement should provide the following information, where applicable:

- Accession codes, unique identifiers, or web links for publicly available datasets
- A description of any restrictions on data availability
- For clinical datasets or third party data, please ensure that the statement adheres to our policy

All RNA sequence data produced in this study can be accessed through the National Center for Biotechnology Center (NCBI) under the BioProject code PRJNA1016074 and Sequence Read Archives (SRA) SRR26046577- SRR26046596. The S. marinoi strains are publicly available from the authors. All other experimental data is available at Zenodo (10.5281/zenodo.10731675). The Swissprot database (https://www.ebi.ac.uk/uniprot/download-center) was downloaded on 2023-04-03. We used the KofamKOALA version of 2023-04-03 (KEGG release 106.0).

Research involving human participants, their data, or biological material

Policy information about studies with human participants or human data. See also policy information about sex, gender (identity/presentation), and sexual orientation and race, ethnicity and racism.

Reporting on sex and gender	NA
Reporting on race, ethnicity, or other socially relevant groupings	NA
Population characteristics	NA
Recruitment	NA
Ethics oversight	NA

Note that full information on the approval of the study protocol must also be provided in the manuscript.

Field-specific reporting

Please select the one below that is the best fit for your research. If you are not sure, read the appropriate sections before making your selection.

☐ Life sciences ☐ Behavioural & social sciences ☒ Ecological, evolutionary & environmental sciences

For a reference copy of the document with all sections, see nature.com/documents/nr-reporting-summary-flat.pdf

Ecological, evolutionary & environmental sciences study design

All studies must disclose on these points even when the disclosure is negative.

Study description	The study tests differences in temperature optima of resurrected diatom strains. Seven strains per time point (1960s, 1990s 2010s) were included in the experiments. To estimate differences in growth optima these strains (n=4) were grown across 6, 8, 10, 14, 18, 20, 22 and 26 degrees Celcius. Potential differences in gene expression patterns between strains from the different time points were tested using three strains from each decade. RNA was extracted from three replicates for each strain (in some cases the RNA yield was too low, in these cases only two replicates were included. Detailed list of RNA samples provided in the Supplementary Information.) We also estimated differences in cell size between the same three strains per time point by measuring their width and length under a microscope.
Research sample	In order to study differences in temperature optima of Skeletonema marinoi we resurrected resting stages from the seafloor in the Archipelago Sea (N Baltic Sea, Finland) originating from different time points {1960s, 1990s, 2010s).
Sampling strategy	In order to include enough intraspecies variability of the strains from within each time point we tested differences in growth and cell size in seven strains across all experimental temperatures. The gene expression patterns were tested using three strains per time point (in total 7 of which 1 was not included because of too low RNA yield) and across three temperature conditions (8, 14 and 20 degrees Celsius).
Data collection	To estimate growth we measured the in vivo fluorescence of chlorophyll a in a 300 µ subsample on a 96-well plate (PerkinElmer, IsoPlate'" 96 F) using a spectrophotometer (Tecan, Infinite® 200 PRO). This was conducted by several authors that are included in the author list. To estimate cell size we used an inverted Olympus IX 51 microscope and a Olympus U-CMAD3 Digital Camera and obtained a minimum of 10 pictures per sample under a 200 x magnification. The width and height of five cells were measured from each picture (Olympus cellSens Dimension imaging software).
Timing and spatial scale	All samples for collecting resting stages were taken in April 2020 from Smaholmen station {60.24N, 22.04E) close to Haverb in the

Timing and spatial scale	Archipelago Sea (N Baltic Sea, Finland). The resting stages were resurrected within the following months the same year. Table S4 specifies all start and end dates of experiments. The chronological dating of the sediment core was conducted by a combination of LOI (Loss on ignition) and 137Cs analysis. The sediment layers that were used in this study dated to the 1960s, 1990s and 2010s (ror range +-2-5 years).
Data exclusions	Strain 46_48_01 was excluded from the RNA-seq analysis because of low RNA yield. Strain 2-4_13 was excluded from all a alyses (also growth rate and cell size analyses) because of contamination. These are specified in Supplementary Table 5.
Reproducibility	Experiments were not repeated. The resurrected strains are kept in cell culture and are publicly available.
Randomization	Resting stages isolated from different layers of the sediment core where allocated into different temporal groups. The temporal groups are based on the chronological /geological dating of the sediment core.
Blinding	Cell size measurements (which are conducted manually) were done blindly to avoid subjective 'measurements'/'choice of cells to m asure 'by the researcher.

Did the study involve field work? ☒ Yes ☐ No

Field work, collection and transport

Field conditions	Field conditions were normal for the month of April in the study area.
Location	60.24N, 22.04E, water depth = 20 meters
Access & import/export	Sample collection from the field was conducted in compliance with local laws.
Disturbance	No significant disturbance was caused during sampling.

Reporting for specific materials, systems and methods

We require information from authors about some types of materials, experimental systems and methods used in many studies. Here, indicate whether each material, system or method listed is relevant to your study. If you are not sure if a list item applies to your research, read the appropriate section before selecting a response.

Materials & experimental systems

n/a	Involved in the study
☒	☐ Antibodies
☐	☒ Eukaryotic cell lines
☒	☐ Palaeontology and archaeology
☒	☐ Animals and other organisms
☒	☐ Clinical data
☒	☐ Dual use research of concern
☒	☐ Plants

Methods

n/a	Involved in the study
☒	☐ ChIP-seq
☒	☐ Flow cytometry
☒	☐ MRI-based neuroimaging

Eukaryotic cell lines

Policy information about cell lines and Sex and Gender in Research

Cell line source(s)	All strains were isolated by the authors and are kept in culture at the corresponding author's laboratory.
Authentication	Only one species of Skeletonema is present in the study area. To 'double-confirm' this we sequenced the 185 rRNA gene for a subset of the strains used in this study.
Mycoplasma contamination	NA
Commonly misidentified lines (See ICLAC register)	NA

Plants

Seed stocks	NA
Novel plant genotypes	NA
Authentication	NA